10 March 2007

Electrode Placement Configurations for 3D EIT

BM Graham[1], A Adler[2]

[1]School of Information Technology and Engineering (SITE), University of Ottawa, Canada
[2]Department of Systems and Computer Engineering, Carleton University, Canada

E-mail: graham.bm@gmail.com, adler@sce.carleton.ca

Abstract. This paper investigates several configurations for placing electrodes on a 3D cylindrical medium to reconstruct 3D images using 16 electrode EIT equipment intended for use with a 2D adjacent drive protocol. Seven different electrode placement configurations are compared in terms of the following figures of merit: resolution, radial and vertical position error, image power, immunity to noise, immunity to electrode placement errors, and qualitative evaluation of image artefacts. Results show that for ideal conditions, none of the configurations considered performed significantly better than the others. However, when noise and electrode placement errors were considered the planar electrode placement configuration (two rings of vertically aligned electrodes with electrodes placed sequentially in each ring) had the overall best performance. Based on these results, we recommend planar electrode placement configuration for 3D EIT imaging of the body.

Keywords: regularization, 3D, EIT, TV Electrical Impedance Tomography

1. Introduction

EIT attempts to calculate a stable and accurate image of the conductivity or conductivity change within a medium from electrical measurements made on the medium boundary. Due to computational complexity, reconstructions have usually been over a 2D Finite Element Mesh (FEM). Continued improvements in computing power have permitted the recent exploration of 3D reconstructions (Metherall 1996, Polydorides 2002). Electrode placement for 2D reconstruction algorithms is confined to planar arrangements that match the 2D reconstruction geometry; yet the EIT problem is inherently 3D as currents cannot be confined to flow in the plane. Consequently 2D reconstructions are subject to artifacts generated by off plane contrasts.

3D reconstruction algorithms with multi-plane electrode arrangements have been used to more accurately reconstruct impedance distributions (Metherall 1996, Polydorides 2002, Vauhkonen *et al* 1997). Dehghani *et al* (2005) investigated *excitation* patterns for applications of 3D breast imaging using 64 electrodes arranged in four layers. Performance was evaluated in terms of singular value decomposition and qualitative evaluation of reconstructed images. Polydorides and McCann (2002) developed and evaluated an electrode segmentation scheme for 3D reconstructions. They examined the effects of the singular values of the Jacobian on the spatial resolution and concluded that the electrode segmentation scheme

significantly improved the conditioning of the Jacobian and resulted in improved resolution.

Many EIT research groups use 16 electrode systems using adjacent stimulation and measurement, based on the original configuration of Barber and Brown (1988a) and Yorkey *et al* (1987). This is the case, for example, of the Goe-MF II adjacent stimulation tomography system (Viasys Healthcare, Höchberg, Germany) available in our lab. With the *adjacent* drive pattern the 16 electrodes are arranged equispaced in a single plane around the perimeter of the medium. Current is applied to an adjacent pair of electrodes and the resultant voltages between the remaining 13 adjacent pairs of electrodes is measured. The three possible measurements involving one or both of the current injecting electrode are not used. This is repeated 16 times with current injected between successive pairs of adjacent electrodes until all 16 possible pairs of adjacent electrodes have been used to apply the known current. This is shown schematically in figure (1). This procedure produces $16 \times 13 = 208$ voltage measurements called

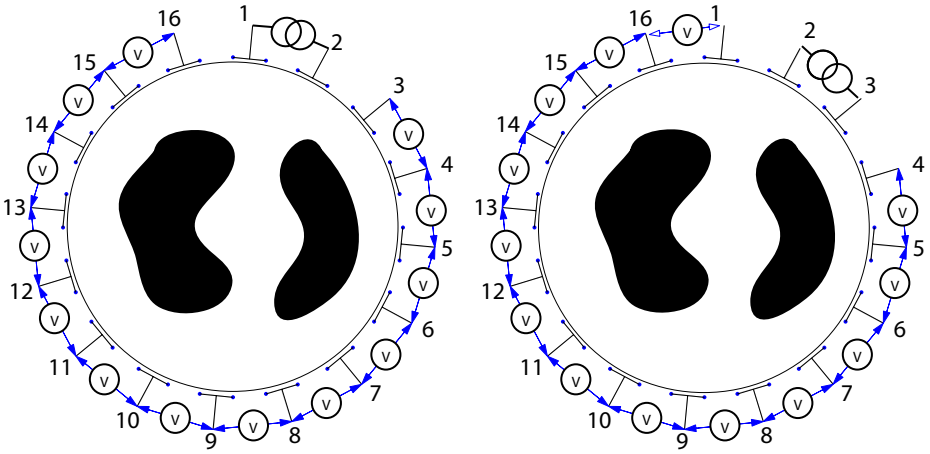

(a) *First of 16 drive pairs* (b) *Second of 16 drive pairs*

Figure 1. *2D Adjacent drive patterns. In figure 1(a) current is injected through electrode pair* $(1, 2)$ *and the resulting boundary voltage differences are measured from electrode pairs* $(3, 4), (4, 5), ..., (14, 15), (15, 16)$. *Voltages are not measured between pairs* $(16, 1), (1, 2)$, *or* $(2, 3)$. *In figure 1(b) the current is injected between pair* $(2, 3)$, *and the voltage differences measured between pairs* $(4, 5), (5, 6), ..., (15, 16), (16, 1)$. *Voltages are not measured between pairs* $(1, 2), (2, 3)$, *or* $(3, 4)$.

an EIT data *frame*. Since the electrodes are numbered 1 through 16 the adjacent pattern in 2D is obtained through a simple *sequencing* of the 16 machine leads to the 16 electrodes. This work is motivated by the desire to use such a 2D system to perform 3D EIT reconstructions.

Compared to 2D there are many more ways to arrange and sequence electrodes when placing them in 3D. Given this variety it is important to know which ones perform best. To answer this question, we evaluate seven EP configurations in which the electrodes are arranged in two parallel planes of eight electrodes each, with electrodes equispaced around the medium. We define an EP configuration as the combination of physical placement of the electrodes and current injection pattern. Different current injection patterns are obtained through various sequencings

or mappings of the 16 electrode leads to electrodes. Performance is evaluated in terms of several figures of merit as well as immunity to noise and performance in the presence of electrode placement errors. These results apply to any medium which is approximately cylindrical; however, we are specifically interested in lung imaging applications, in which one wants to obtain more accurate tomographic slices throught the chest.

2. Methods

We consider EIT difference imaging, which is widely understood to improve reconstructed image stability in the presence of problems such as unknown contact impedance, inaccurate electrode positions, nonlinearity, and in the 2D case, the use of 2D approximations for 3D electrical fields (Barber and Brown 1988, Lionheart 2004). We address the class of normalized one-step linearized reconstruction algorithms that calculate the change in a finite element conductivity distribution, $\boldsymbol{x} = \boldsymbol{\sigma}_2 - \boldsymbol{\sigma}_1$ due to a change in EIT difference signal, $\mathbf{z} = \mathbf{v}_2 - \mathbf{v}_1$ over a time interval (t_1, t_2). By convention we consider the signal at t_1 to be the *reference* frame and the signal at t_2 to be the *data* frame. Since we do not know $\boldsymbol{\sigma}_1$, $\mathbf{x}$ is interpreted as the change in conductivity with respect to the unknown initial conductivity $\mathbf{x} = \Delta\boldsymbol{\sigma} = \boldsymbol{\sigma}_2 - \boldsymbol{\sigma}_1$.

For small changes around a background conductivity the relationship between $\mathbf{x}$ and $\mathbf{z}$ may be linearized as

$$\mathbf{z} = \mathbf{H}\mathbf{x} + \mathbf{n} \tag{1}$$

where $\mathbf{H}$ is the Jacobian or sensitivity matrix and $\mathbf{n}$ is the measurement system noise, assumed to be uncorrelated additive white Gaussian (AWGN). Each element i, j, of $\mathbf{H}$ is calculated as $\mathrm{H}_{ij} = \left.\frac{\partial \mathrm{z}_i}{\partial \mathrm{x}_j}\right|_{\sigma_0}$ and relates a small change in the i^{th} difference measurement to a small change in the conductivity of j^{th} element. $\mathbf{H}$ is a function of the FEM, the current injection pattern, and the background conductivity. We use a homogenous background conductivity in which $\boldsymbol{\sigma}_0 = \mathbf{1}$ for each of the elements.

2.1. Image Reconstruction

In order to overcome the ill-conditioning of $\mathbf{H}$ we solve (1) using the following regularized inverse

$$\hat{\mathbf{x}} = (\mathbf{H}^\mathbf{T}\mathbf{W}\mathbf{H} + \lambda^2\mathbf{R})^{-\mathbf{1}}\mathbf{H}^\mathbf{T}\mathbf{W}\mathbf{z} = \mathbf{B}\mathbf{z} \tag{2}$$

where $\hat{\mathbf{x}}$ is an estimate of the true change in conductivity distribution, $\mathbf{R}$ is a regularization matrix, λ is a scalar hyperparameter that controls the amount of regularization, and $\mathbf{W}$ models the system noise. Since noise is uncorrelated in the system, $\mathbf{W}$ is a diagonal matrix with $\mathbf{W}_{ii} = 1/\sigma_i^2$ where σ_i^2 is the noise variance for measurement i. $\mathbf{W}$ can also be modified to account for variable gain settings on each tomograph channel. However, for this work we assume that all measurements have equal noise variance with the result that $\mathbf{W}$ becomes a multiple of the identity matrix.

In this work we use $\mathbf{R} = diag(\mathbf{H}^\mathbf{T}\mathbf{H})$ which is the regularization matrix used in the NOSER algorithm of Cheney *et al* (1991). Hyperparameter selection was performed using the *BestRes* method (Graham and Adler 2006a) extended for 3D as described in Graham and Adler (2006b).

Solution of (2) for 3D requires solving linear systems that are too large to be solved with linear algebra systems based on 32 bit pointers (such as is available in

current versions of Matlab). Graham and Adler (2006b) describe a *Nodal Jacobian* inverse solver algorithm that converts the element based Jacobian of equation (2) to a nodal based Jacobian. This algorithm reduces the size of $\mathbf{H^T WH}$ by up to a factor of 36 (the improvement factor for the model used in this work is 26.15) and allows the solution of Finite Element Models with 21000 elements and over 4000 nodes such as those used in this work ‡

2.2. Finite Element Models

Simulated data were generated from a dense 28 layer, 86016 element, 15805 node FEM mesh, while reconstructions were performed on a coarser 28 layer, 21504 element, 4205 node mesh. Both meshes matched the geometry of the 28cm diameter by 28cm high cylindrical tank in our lab which can be used with the Goe-MF II type tomography system. Thus each layer was 1cm thick. Electrodes were 2.8cm by 1cm in size and arranged in two parallel planes 11cm apart which can be seen in figure 2. The lower plane of electrodes are located in the 9^{th} layer (z=8 to z=9cm), while the upper plane of electrodes are located in the 20^{th} layer (z=19 to z=20cm). Figure 3 shows the dense mesh while figure 2 shows the coarse meshes.

2.2.1. Electrode Placement Configurations With 2 layers of electrodes the 16 electrode leads can be connected to the 16 tank electrodes in an arbitrary way that we call a sequence. We call the combination of electrode *arrangement* on the tank (either aligned or offset in this work) and *sequencing* an *Electrode Placement (EP) configuration*. The following 7 EP configurations are proposed and evaluated in this paper: Planar, Planar-Offset, Planar-Opposite, Zigzag, Zigzag-Offset, Zigzag-Opposite, and Square. Table 1 provides a mapping of the 16 sequentially numbered electrodes, indicated in figure 1, to the 16 physical tank locations which are identified by letter on figures 2(a) and 2(b).

For the three Planar EP configurations, measurements are mainly taken between electrodes in the same plane (intra-planar), with the exception of measurements taken between electrodes 8 & 9, and 16 & 1 which are inter-planar measurements. With the three Zigzag patterns measurements are always taken between electrodes in different planes (inter-planar). The Square EP configuration has an equal amount of data taken from inter- and intra-planar electrode pairs.

2.3. Evaluation Procedure

The seven EP configurations were evaluated using three simulation experiments for each configuration: vertical target movement, radial target movement, and contrast discrimination. For each of the seven EP configurations a single homogenous reference frame was simulated using the dense FEM shown in figure 3. The vertical target movement experiment consisted of data frames generated using a small target located halfway along the radius of the tank (r/2) that was moved through 28 vertical positions as illustrated by the vertical stack of (green) elements indicated in figure 3. The radial target movement experiment consisted of data frames generated using a small target located at the midplane of the figure 3 tank (a height of 14 cm) that was moved

‡ The work discussed in this paper was developed with the EIDORS Version 3 (Adler and Lionheart, 2006) package using the complete electrode model (Vauhkonen *et al* 1997). Software for this work is currently being added to EIDORS; this will be complete by Jan 2007.

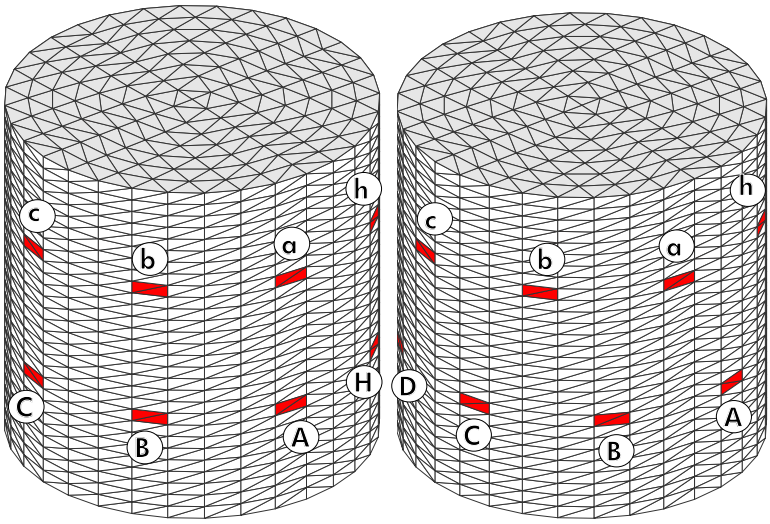

(a) *Aligned* (b) *Offset*

Figure 2. *Meshes used for reconstruction. Figure 2(a) is the* aligned *electrode arrangement. Figure 2(b) is the* offset *electrode arrangement. With the* offset *arrangement the lower electrode plane is rotated such that the electrodes are offset by half the inter-electrode spacing.*

Aligned, fig 2(a)	Planar	Zigzag		Zigzag-Opposite	Square
Offset, fig 2(b)	Planar-Offset	Zigzag-Offset	Planar-Opposite		
1	a	a	a	a	a
2	b	B	E	e	b
3	c	b	b	b	B
4	d	C	F	f	C
5	e	c	c	c	c
6	f	D	G	g	d
7	g	d	d	d	D
8	h	E	H	h	E
9	A	e	e	D	e
10	B	F	A	H	f
11	C	f	f	C	F
12	D	G	B	G	G
13	E	g	g	B	g
14	F	H	C	F	h
15	G	h	h	A	H
16	H	A	D	E	A

Table 1. *Mapping of electrode number to tank location (letter) for the seven EP configurations. First column is electrode lead number, other columns are corresponding electrode position on tank as shown in 2.*

from the centre to the side of the mesh in 14 steps along the radius. The contrast discrimination experiment consisted of data frames generated using two small targets: a conductivity decrease located vertically at a height of 14cm, at a radial distance

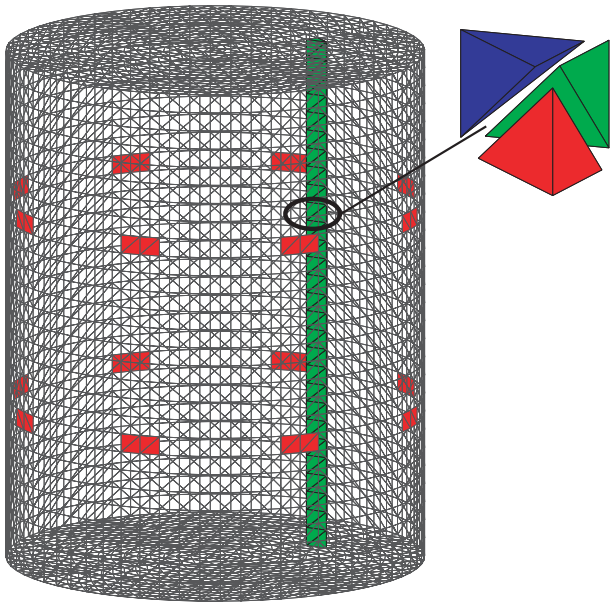

Figure 3. *The r/2 impulse was generated from a three tetrahedron wedge taken from each of the 28 layers of the large mesh. This produced 28 data frames per EP configuration. Lower electrode plane is at z=8 to z=9cm. Upper electrode plane is at z=19 to z=20cm.*

of r/2 at 3 o'clock and a conductivity increase located vertically at height 4cm, at a radial distance of r/2 at 9 o'clock (opposite side of tank).

Subsequently, for each of the seven EP configurations, 28 reconstructions were calculated for the vertical target movement experiment and 14 reconstructions were calculated for the radial target movement experiment under various conditions of noise and electrode placement errors. A single reconstruction was made for each of the EP configurations for the contrast discrimination experiment. Two planes of electrodes lead to a logical partitioning of the tank into three zones (top and bottom end zones, and the middle zone). It is assumed that in many cases the region of interest (ROI) will be confined to the middle zone. A good EP configuration will minimize reconstruction artefacts in the middle zone caused by contrasts in the end zones.

Reconstructions were evaluated and compared based on the following criteria:

(i) *SNR and Conditioning*: The SNR of the difference signals for each configuration were compared. We define SNR $= 20\log_{10}\text{mean}(\mathbf{z})/\text{stdDev}(\mathbf{z})$. The condition numbers and singular values of each Jacobian matrix were compared: the SVD of a matrix $\mathbf{H}$ is a decomposition of the form

$$\mathbf{H} = \mathbf{U}\Sigma\mathbf{V}^T = \sum_{i=1}^{N} \mathbf{u}_i \sigma_i \mathbf{v}_i^T$$

where $\mathbf{U} = (\mathbf{u}_1, ..., \mathbf{u}_n)$ and $\mathbf{V} = (\mathbf{v}_1, ..., \mathbf{v}_n)$ are matrices with orthonormal columns, $\mathbf{U}^T\mathbf{U} = \mathbf{V}^T\mathbf{V} = \mathbf{I}_n$, and where Σ is a diagonal matrix with non-negative diagonal elements, σ_i arranged in non-increasing order such that $\sigma_1 \geq ... \geq \sigma_n \geq 0$. The σ_i are the singular values of $\mathbf{H}$. The condition number of $\mathbf{H}$ is $cond(\mathbf{H}) = \sigma_1/\sigma_n$.

(ii) *Resolution* is a figure of merit (FOM) defined in terms of the 3D extension of the blur radius measure used in Adler and Guardo (1996). For 3D BR is defined as $BR = r_z/r_0 = \sqrt[3]{V_z/V_0}$ where r_0 and V_0 are the radius and volume respectively of the entire 3D medium and r_z and V_z are the radius and volume of the reconstructed contrast containing half the magnitude of the reconstructed image. BR calculates the volume fraction of the elements that contain the largest amplitude contributions to 50% of the total image amplitude. It is a measure of the concentration of image amplitude. The set of elements that contribute to the blur radius is called the half amplitude (HA) set (Graham and Adler 2006a).

(iii) *Radial Position Error (PE)* is a FOM defined as the proportional difference in radial position of the centre of mass of the reconstructed image HA set and the centre of mass of the generating small target. This is expressed as a percentage where a negative quantity indicates that the reconstructed image is closer to the centre of the tank then the corresponding generating impulse.

(iv) *Vertical PE* is a FOM defined as the proportional difference in the vertical position of the centre of mass of the reconstructed image HA set and the centre of mass of the generating small target. This is expressed as a percentage of tank height where a negative quantity indicates that the reconstructed image is closer to the central plane of the tank then the corresponding generating impulse.

(v) *Image Magnitude (IM)* is a FOM that measures the magnitude of the HA set. It is defined as the sum of the volume-weighted element conductivity magnitudes where the only elements of the HA set are included: $IM = \sum_{i \in HA} ||\sigma_i||V_i$ where V_i is the volume of the i^{th} element, σ_i is the estimated change in conductivity of the i^{th} element.

(vi) *Qualitative Evaluation* of reconstructed images which is primarily a subjective evaluation of image artifacts. We expect a qualitatively good image to appear as a small spherical blur corresponding to the generating target. A poor image could exhibit artefacts such as non-spherical extent, features that exist in the wrong locations or that do not correspond to the generating target, and protrusions from the main image.

(vii) *Immunity to Noise.* Using the vertical target movement data, an additional six sets of reconstructions were calculated for each of the seven EP configurations in which AWG noise was added in six steps from 0.1% to 0.6% of the difference signal, $\mathbf{z}$. The ability of each EP configuration to reconstruct images in the presence of this noise was then compared in terms of the FOMs described earlier.

(viii) *Immunity to systematic electrode placement errors.* Two techniques were used to evaluate electrode position errors.

(a) In the first technique reconstructions were performed with a systematic electrode position error in which data collected with one of the EP configurations was reconstructed using the same electrode sequence but with the lower plane of electrodes rotated by half the inter-electrode distance (*Offset-Error*). Thus in this first case data generated with the Planar EP configuration was reconstructed using the Planar-Offset EP configuration. This is shown in figure 4 direction A. In the second case data generated with the Planar-Offset EP configuration was reconstructed using the Planar EP configuration. This is shown in figure 4 direction B. In the case of pulmonary imaging this error simulates a twisting of the thorax.

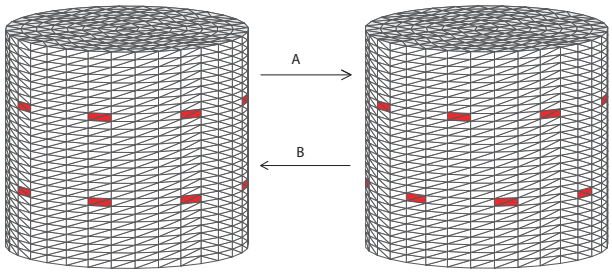

Figure 4. *Offset Error. Direction A: Data observed with aligned arrangement were reconstructed with offset arrangement. Direction B: Data observed with offset arrangement were reconstructed with aligned arrangement*

(b) In the second technique an *Electrode Plane Separation Error* was evaluated as follows: For each EP configuration 9 sets of data were simulated with the distance between the electrode planes increasing from the correct separation of 11cm, to a layer separation of 20cm. Each set was comprised of homogenous reference frame and 28 data frames generated with a small target as in section 2.3. Each of 9 data sets per EP configuration was then reconstructed on the same mesh geometry but always with the electrodes at the interplanar distance of 11cm. This simulates a systematic electrode placement error in which the reconstruction model does not match the actual electrode placement for 8 of the 9 simulated data sets. In the case of pulmonary imaging this error simulates an inaccurate application of the electrodes.

3. Results

In this section, we compare each EP strategy against each figure of merit, in order to differentiate amongst the performance of the various EP configurations.

Evaluation of Maximum Performance Experiments. The initial evaluation looked at the best case performance of the EP configurations in that noise was not added to the vertical or radial movement data described in section 2.3 nor were electrode errors present. The following observations were made concerning this best case set of reconstructions:

- SNR and Conditioning: The normalized SNR is listed in table 2. The Planar and Planar-Offset EP configurations have similar and significantly larger SNRs than the other configurations. This indicates that these two configurations should be more robust to noise than the others. This is observed in section 3 - Evaluation of Noise Effects. The condition numbers are also listed in table 2 but are less informative. Although there is a difference of a factor of 10 between the Square and Planar-Opposite configurations this is not significant in that all of the condition numbers are in excess of 10^{22}.
  The singular values of each Jacobian were calculated for each EP configuration and are plotted in figure 5. Also included are the singular values for the 2D EP configuration in which the 16 electrodes are arranged in a single plane. The long term trend of the singular values is not significantly different between the

EP Configuration	SNR (normalized)	SNR (db)	cond($\mathbf{H}^T\mathbf{H}$) ($\times 10^{23}$)
Planar	1.0000	-3.9568	0.7826
Planar-Offset	0.9709	-4.0849	3.8234
Planar-Opposite	0.3852	-8.0997	0.4019
Zigzag	0.2965	-9.2365	2.0639
Zigzag-Offset	0.2702	-9.6406	2.6358
ZigZag-Opposite	0.2924	-9.2971	0.6721
Square	0.3907	-8.0380	5.8860

Table 2. *Comparison of EP Configurations in terms of SNR and Jacobian Condition Number.*

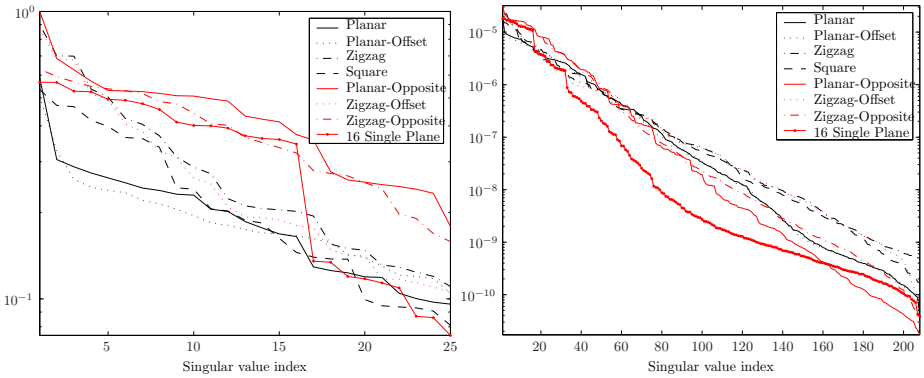

(a) *First 25 Singular Values, normalized* (b) *All Singular Values, non-normalized*

Figure 5. *Singular Values of* $\mathbf{H}$ *for the 7 EP Configurations*

various EP configurations with the exception of the 2D configuration. Figure 5(a) shows the first 25 singular values, in this case normalized to the first and largest singular value. Although there are variations in the singular values the long term trends are similar and we conclude in this case that the singular values are not useful discriminators of the seven EP configurations. Picard plots of all EP configurations are similar; the Picard condition is satisfied for each EP configuration, however the singular values never cross the Picard coefficients. Thus it is not possible to use Picard plots to determine the number of singular values above the noise.

- Resolution: Figure 6(a) shows Resolution as a function of reconstructed height. The resolution of all EP configurations varies as a function of the height of the contrast. The resolution curves of figure 6(a) show that the range of variation in resolution amongst the EP configurations, in the end regions is large compared to the range of variation in the middle section. The Planar EP configuration has the best resolution in the end zones, the opposite configurations have the worse performance in the middle zone; however, the differences are small and it appears that Resolution is not a strong discriminator of EP configurations. In general the resolution of all EP configurations varies as a function of distance from electrode plane so none of the EP configurations have a stable resolution vs contrast height function; however, the relative magnitude of the instability is small.

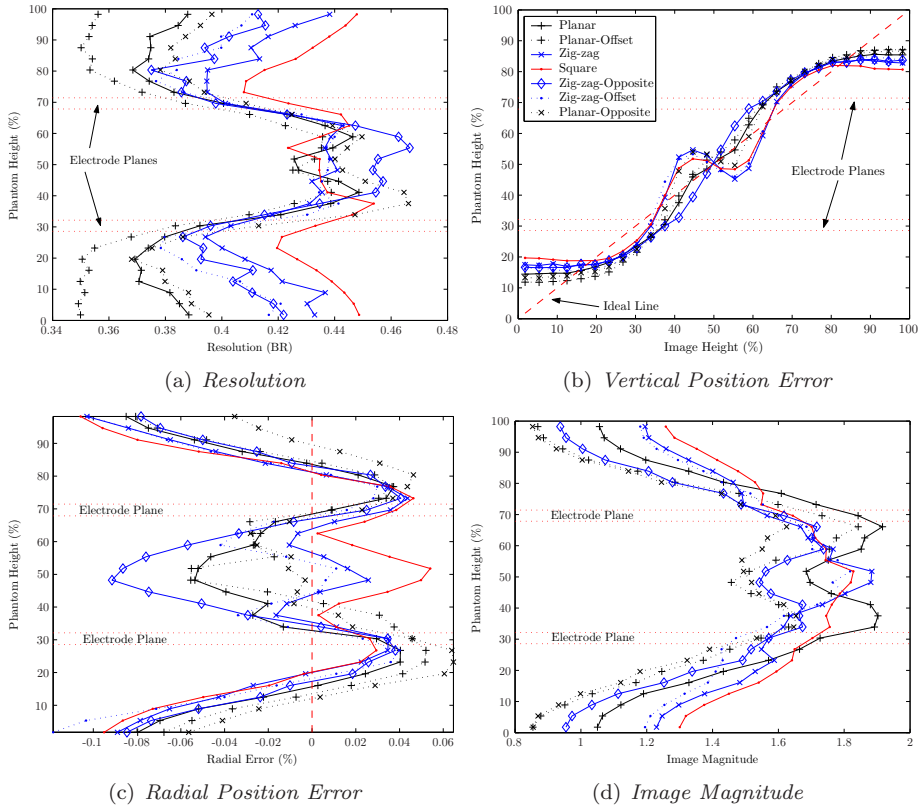

(a) *Resolution* (b) *Vertical Position Error*

(c) *Radial Position Error* (d) *Image Magnitude*

Figure 6. *Performance measures for 7 EP Stategies vs Contrast Height for noise free reconstructions of a contast moving through 28 vertical positions at $r/2$. Legend in figure 6(b) is for all plots.*

- Vertical PE: Figure 6(b) shows Vertical PE vs reconstructed height. For perfect reconstructions the curves would be straight lines. All of the EP configurations suffer from a vertical range compression in the end sections. The Zigzag, Zigzag-Offset, Square, and Planar-Opposite EP configurations have a large non-linearity in the central region of the graph. This is undesirable as it causes the reconstruction to be unstable; a small change in the vertical position of the generating contrast can cause a large change in the vertical position of the reconstruction. A good EP configuration should have a near linear response in the middle zone. Vertical PE is an useful discriminator of EP configurations.
- Radial PE: Figure 6(c) shows that for all of the EP configurations Radial PE is largest at the ends, improves as the generating contrast approaches the electrode planes, and decays as the contrast moves between the electrode planes. The various Radial PE curves behave differently in the inter-planar region; however, the difference is mainly one of sign with the magnitudes being small. Radial PE is not a strong discriminator of EP configurations.
- Image Magnitude: Figure 6(d) is a plot of Image Magnitude vs phantom height showing that Image Magnitude increases as the phantom location moves from the ends of the tank toward the electrode planes. Although the behaviour of the

various EP configurations in the middle section is different for each configuration it is difficult to say what behaviour is desired and therefore which EP configuration is preferable. Overall, Image Magnitude is not a strong discriminator of EP configurations.

- Radial Performance: Figure 7 shows various performance measures for reconstructions from the radial movement data. As expected, the resolution

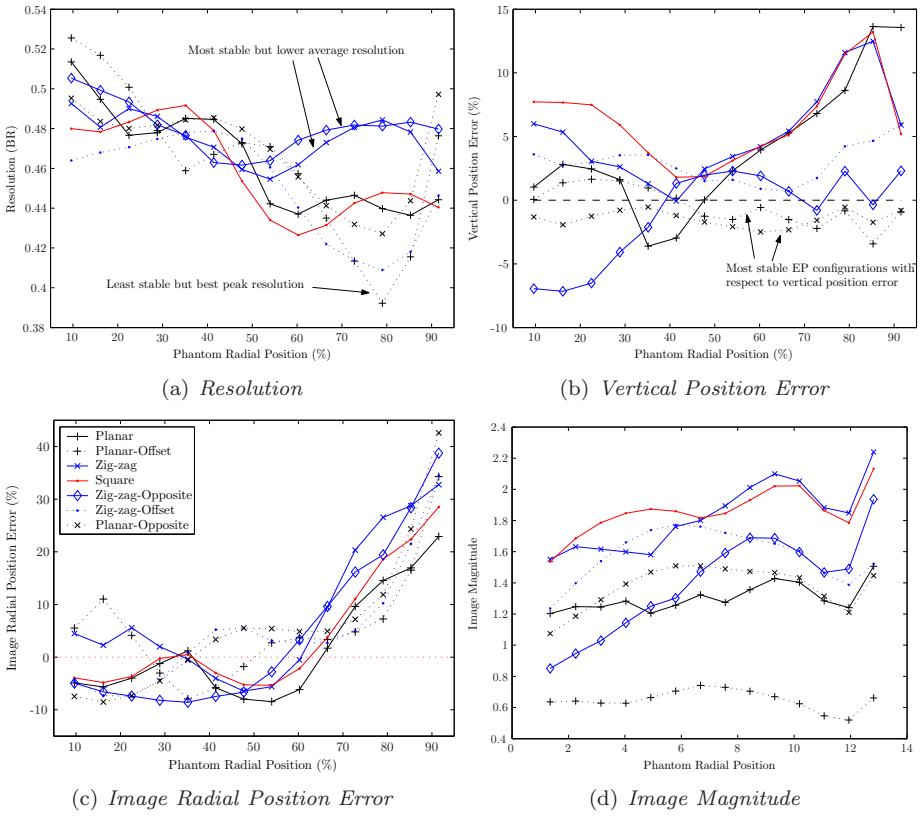

(a) *Resolution* (b) *Vertical Position Error*

(c) *Image Radial Position Error* (d) *Image Magnitude*

Figure 7. *Performance measures for 7 EP Stategies vs Contrast Radial Position for noise free reconstructions of a contast moving through 14 radial positions at the vertical centre of the tank. Legend in figure 7(c) is for all plots.*

plot of figure 7(a) shows a large variability in resolution as a function of radial position for all the EP configurations. The Zigzag and Zigzag-Opposite EP configurations have the most stable response albeit at a lower average resolution while the Planar-offset and Zigzag-offset configurations show the most variability in resolution yet have the best peak resolution (at the 80% radius). Figure 7(b) shows a large variability in vertical position error for all EP configurations with the exception of the Planar-Opposite, and Planar-Offset configurations which are relatively stable. Image radial position error, figure 7(c), is similar for all configurations thus is a poor discriminator for the set of configurations being evaluated. Finally, figure 7(d), indicates that image magnitude of the Planar and Planar-offset EP configurations are marginally more stable than the other configurations; however, image magnitude does not appear to be a strong

discriminator between configurations.

- Qualitative Evaluation: Figure 8 shows several reconstructions for contrasts located at the centre plane of the tank. The Planar, Planar-Opposite, Planar-Offset and Square EP configurations, figure 8(a), produce circular reconstructions that are all circular/spherical. The Zigzag figure 8(b) and Zigzag-Opposite figure 8(c) configurations produce images that are vertically elongated while the reconstruction of the Zigzag-Offset EP configuration figure 8(d) is banana shaped. Additionally the Zigzag-Opposite configuration figure 8(c) has "finger" like artefacts extending from the image to the electrode planes. The best performance for targets located in the end sections are obtained with the Zigzag and Square EP configurations while reconstructions using the Planar, Planar-Offset (similar) and Planar-Opposite EP configurations produce images with large artifacts. As mentioned in section 2.3, in some applications the region of interest (ROI) may be confined to the middle zone in which case it may be preferable to use an EP configuration that works very well in the ROI despite producing artifacts for contrasts located in the end zones.

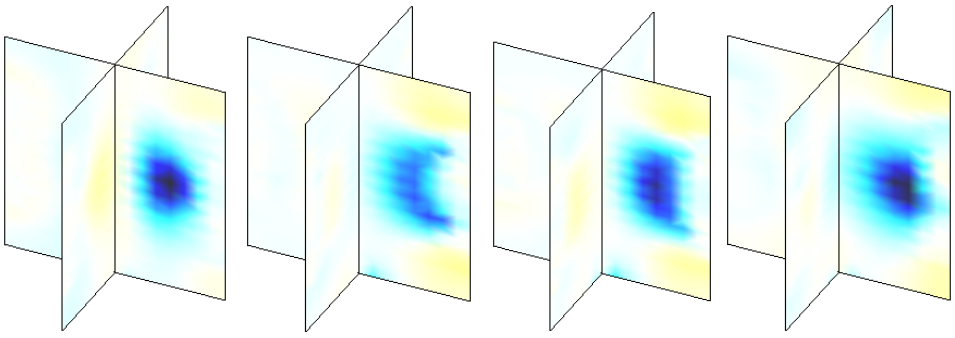

(a) *Planar-Offset, Planar, Planar-Opposite, and Square are similar.* (b) *Zigzag-Offset* (c) *Zigzag* (d) *Zigzag-Opposite*

Figure 8. *Baseline reconstructions for the $r/2$ small target at midplane ($z = 14cm$).*

- Contrast Discrimination: Figure 9 show vertical slices through the mesh for 3D reconstructions of the contrast discrimination experiment data. All of the 3D EP configurations are able to localize the two contrasts as shown in figures 9(a) to 9(c). The Square and Zigzag-Offset EP configurations, figure 9(a), provide the best qualitative performance in terms of section 2.3(vi); however, the Planar, Planar-offset and Zigzag EP configurations, which are similar in appearance to each other, figure 9(b), are almost as good. Of the 3D EP configurations, the Planar-opposite is clearly the worst performer with the lower phantom being quite blurred, figure 9(c). Figure 9(d) shows that the 2D electrode arrangement cannot accurately locate the contrasts: the centrally located phantom appears as a conductivity decrease image with a large vertical extent and a crescent shape centred in the mesh while the phantom located at 4cm height is also reconstructed as a large crescent shape centered through the middle of the mesh.

Evaluation of Noise Effects. In addition to the baseline reconstructions

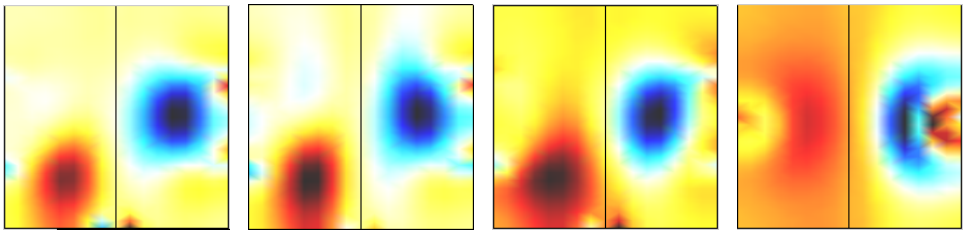

(a) *Square* *Zigzag-Offset,* (b) *Planar, Zigzag, Planar-Offset* (c) *Planar-Oposite* (d) *2D Adjacent*

Figure 9. *2D slices taken vertically through the centre of the reconstruction mesh showing 3D localization of contrasts.*

discussed above, an additional six sets of reconstructions were calculated for each of the seven EP configurations in which AWG noise was added in six steps from 0.1% to 0.6%. The noise was added to the data simulated as described in section 2.3. The Zigzag and Zigzag-Offset EP configurations could not produce useful reconstructions for noise levels above 0.2% while the Square EP configuration did not work with noise above 0.3%. Although useful reconstructions could be calculated using the two Opposite EP configurations with up to 0.6% noise, their Resolution and PE performance degraded rapidly. The Planar and Planar-Offset EP configurations were very robust to noise; resolution and PE degraded slowly and good images were reconstructed with noise in excess of 0.6%.

Electrode Position Errors - Offset Error. All of the EP configurations suffered degradation in resolution due to the offset error. The Zigzag-Offset pattern has the largest loss of resolution; however, the Planar-Opposite EP configuration gave the worse overall performance: a conductivity decrease resulted in images of a conductivity increase. The Planar, Planar-Offset, and Zigzag EP configurations were able to reconstruct a circular/spherical image without introducing image shape artifacts. In all cases the centre of mass of the reconstructions were rotated in the axial plane by about 20°. Since EIT is expected to be used for functional imaging as opposed to anatomical imaging, the rotation position error may not be important as long as the magnitude of the conductivity change is accurate.

Electrode Position Errors - Electrode Plane Separation Error. Radial PE, Vertical PE and Resolution are not significantly affected by electrode plane sepearation errors for any of the EP configurations. All of the performance measures degraded smoothly. This can be seen with some representative plots in figures 10(a) to 10(c). Qualitatively, all configurations produced vertically elongated images with the Square and the two Opposite EP configurations being most affected, Zigzag and Zigzag-Offset configurations less so, and the Planar and Planar-Offset EP configurations the least. For contrasts located in the end zones, the Zigzag, Zigzag-Offset, and Square configurations show a swirling artifact while the Opposite EP configurations show an extensive vertical lengthening of the reconstructed contrast. The Planar and Planar-Offset EP configurations also showed an increased Radial PE due to the contrast being *pushed* toward the tank centre for phantoms located in the end sections. This effect was less noticeable with the Planar EP configuration. Both the Planar and Planar-Offset EP configurations show little degradation due to electrode plane separation errors of up 20% (6cm on the 28cm tall tank). The Planar-

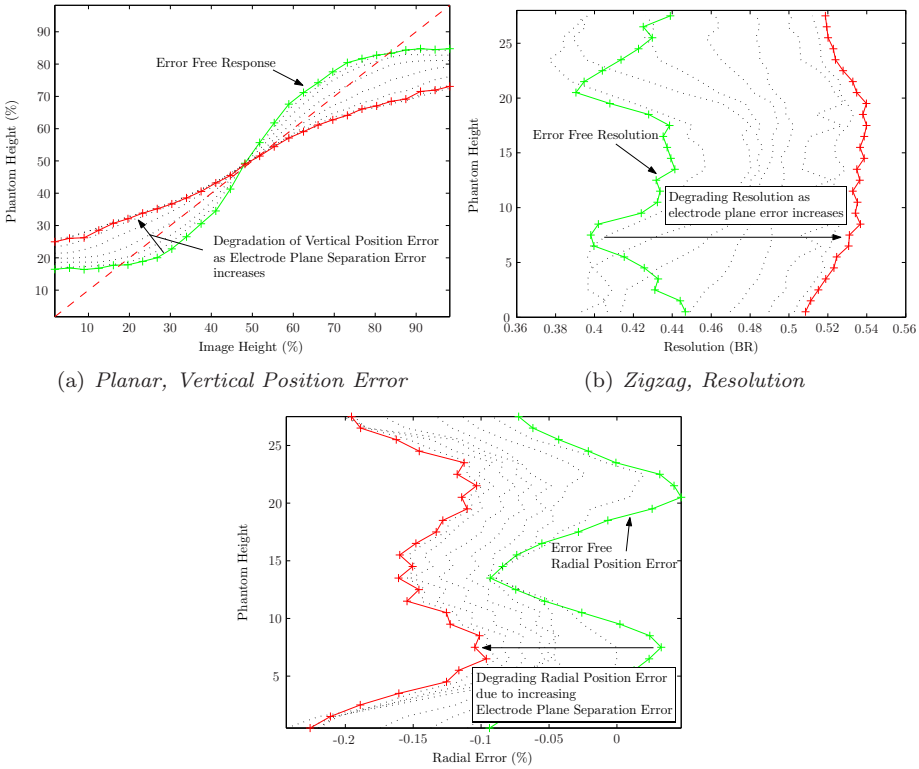

(a) *Planar, Vertical Position Error*

(b) *Zigzag, Resolution*

(c) *Planar-Opposite, Radial Position Error*

Figure 10. *Degradation of selected performance measures for selected configurations due to electrode plane separation error. The Error Free curves represent no electrode plane separation error. The dotted curves represent increasing electrode plane separation to a maximum of 10 cm error represented by the red solid line.*

Offset is slightly more robust than the Planar EP configuration in this regard.

2D Limitations. In addition to the seven 3D EP configurations additional reconstructions were performed using the same 3D meshes but with the 16 electrodes arranged in a single plane at a height of 14cm. The plots of figure 11 were generated similarly to those of section 2.3: 28 data frames from the $r/2$ phantom moving through 28 vertical locations. Figure 11(c) validates the obvious insight that vertical position cannot be resolved using a single plane of electrodes. Regardless of actual phantom height, the 2D arrangement always reconstructs an image that is located in the plane of the electrodes. As the small target moves farther away from the electrode plane the resolution, figure 11(a), and the image magnitude, figure 11(d), both decrease while the the radial error, figure 11(b), increases.

Summary. A qualitative summary of the significant discriminators is presented in table 3. Five of the configurations show poor performance in one or more of the discriminators while the Planar and Planar-offset configurations, which have similar performance, do not.

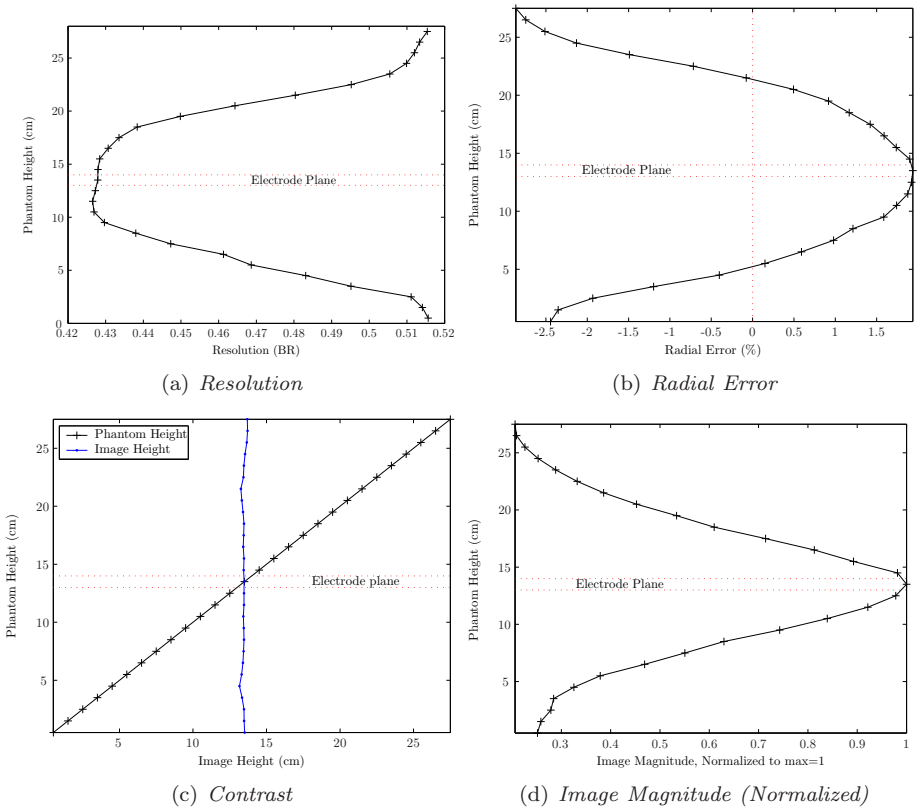

(a) *Resolution* (b) *Radial Error*

(c) *Contrast* (d) *Image Magnitude (Normalized)*

Figure 11. *Performance measures vs Phantom Height for noise free reconstructions with single layer of 16 electrodes for the small target moving through 28 vertical positions at $r/2$.*

Figure of Merit Reference	Res Fig 6(a)	VPE Fig 6(b)	Qual Sect 3	Noise Sect 3	Offset Err Sect 3	Sep Err Sect 3	VPE (Radial) Fig 7(b)
Planar			+	+	+	+	
Planar-Offset			+	+	+	+	+
Planar-Opposite	-		+		- -	- -	+
Zigzag		- -	-	- -	+	-	
Zigzag-Offset		- -	- -	- -	-	-	
ZigZag-Opposite	-		-			- -	
Square		- -	+	-		- -	

Table 3. *Comparison Summary of EP Configurations - in the ROI.*

4. Conclusion

This paper has investigated the performance of a small set of 3D electrode placement configurations under the constraints of a 16 electrode adjacent drive system intended for 2D applications. We make the following observations:

(i) Opposite EP configurations are highly susceptible to corruption by noise and are not recommended.

(ii) The Zigzag EP configuration performs poorly in the presence of noise.

(iii) The Zigzag-Offset EP configuration is susceptible to Offset error.

(iv) The Square configuration suffers from the instability in VPE, has poor noise performance, and shows electrode to contrast "finger" artifacts.

(v) The Planar and Planar-Offset EP configurations are most robust to noise and systematic electrode placement errors and have performance as good or better than the other configurations for targets in the ROI.

(vi) The Planar EP configuration provides the largest image power for contrasts located in the centre section, and is the most robust to noise (slightly better than Planar-offset).

Our results suggest that no one EP configuration offers a worthwhile improvement over the others under ideal conditions. This observation that there is little difference in the noise free cases may be attributable to the fact that the various patterns are linearly dependent; thus given noise free data, it is possible to calculate any set from any other. Only when noise and electrode placement errors are considered does the choice of EP configuration become important.

The difficulty of placing electrodes accurately on a person may be the largest discriminating factor amongst EP configurations intended for clinical use. Moreover electrode placement errors are exacerbated and change throughout the imaging session due to subject movement. This leads one to prefer an EP configuration that is robust to electrode placement errors and is easy to apply on a patient.

In summary, the goal of this paper was to evaluate a electrode placement strategies for 16 electrode adjacent drive EIT systems in order perform 3D image reconstructions. Based on the results, and considering the value of easy of electrode placement, we recommend Planar electrode placement. Thus, 16 electrodes should be placed in two rings of vertically aligned electrodes with electrodes placed sequentially in each ring.

References

Adler A and Guardo R 1996 Electrical impedance tomography: regularised imaging and contrast detection *IEEE Trans. Med. Imaging* **15** 170-9

Adler A and Lionheart WRB 2006 Uses and abuses of EIDORS: An extensible software base for EIT *Physiol Meas* **27** S25-S42

Barber DC 1989 A review of reconstruction techniques for electrical impedance tomography *Med Phys* **16** 162-169

Barber DC and Brown BH 1988a Single step Algorithms for Image reconstruction *IEEE Trans Biomedical Engineering* **32** 100-105

Barber DC and Brown BH 1988 Errors in reconstruction of resistivity images using a linear reconstruction technique, *Clin Phys Physiol Meas* **9** 101-4

Cheney M, Isaacson D, Newell JC, Simske S and Goble JC 1991 NOSER: an algorithm for solving the inverse conductivity problem *Int. J. Imaging Syst. Technol* **2** 66-75

Dehgani H, Soni N, Halter R, Hartov A, Paulsen KD 2005 Excitation patterns in three-dimensional electrical impedance tomography *Physiol. Meas.* **26** S185-S197

Graham BM and Adler A 2006a Objective Selection of Hyperparameter for EIT *Physiol. Meas.* **27** S65-S79

Graham BM and Adler A 2006b A Nodal Jacobian Inverse Solver for Reduced Complexity EIT Reconstructions *Int. J. for Information & Systems Sciences* **2** 453-68

Lionheart WRB 2004 Review: Developments in EIT reconstruction algorithms: pitfalls, challenges and recent developments *Physiol Meas* **25** 125-142

Metherall P, Barber DC, Smallwood RH and Brown BH 1996 Three dimensional electrical impedance tomography *Nature* **380** 509-12

Polydorides N 2002 Image reconstruction algorithms for soft-field tomography *PhD Thesis* UMIST

Polydorides N and McCann H 2002 Electrode configurations for improved spatial resolution in electrical impedance tomography *Meas. Sci. Technol.* **13** 1862-1870

Vauhkonen M, Kaipio JP, Somersalo E and Karjalainen PA 1997 Electrical impedance tomography with basis constraints *Inverse Problems* **13** 523–30

Yorkey TJ, Webster JG, Tompkins WJ 1987 Comparing reconstruction algorithms for electrical impedance tomography *IEEE Trans Biomed Eng* **BME-34** 843-852